Microelectronics Reliability 74 (2017) 165–172

Contents lists available at ScienceDirect

Microelectronics Reliability

journal homepage: www.elsevier.com/locate/microrel

Towards prognostics and health monitoring: The potential of fault detection by piezoresistive silicon stress sensor

Alicja Palczynska [a,*], Alexandru Prisacaru [a], Przemyslaw Jakub Gromala [a], Bongtae Han [b], Dirk Mayer [c], Tobias Melz [c]

[a] Robert Bosch GmbH, Reliability Modeling and System Optimization (AE/EDT3), Reutlingen 72703, Germany
[b] Mechanical Engineering Department, University of Maryland College Park, MD 20742, USA
[c] Fraunhofer-Institut für Betriebsfestigkeit und Systemzuverlässigkeit LBF, Darmstadt 64289, Germany

ARTICLE INFO

Article history:
Received 8 September 2016
Received in revised form 22 March 2017
Accepted 10 April 2017
Available online 5 May 2017

ABSTRACT

A piezoresistive silicon based stress sensor has been demonstrated successfully as an effective tool to monitor the stresses inside electronic packages during various production processes. More recently, the sensor has been evaluated as a sensor for Prognostics and Health Monitoring (PHM) systems. This paper presents a systematic approach that evaluates its performance from the perspective of failure mode detection. A detailed Finite Element method (FEM) model of existing test vehicles is created. The test vehicle consists of six DPAK (Discrete Package) power packages and three stress sensors. The results of simulation are verified by the signals obtained from the stress sensor as well as the supplementary warpage measurements. After inserting various failure modes into the model, statistical pattern recognition algorithms are implemented for fault detection and classification. The proposed technique can identify detectable failures during reliability testing by utilizing the database of stress sensor responses for healthy and unhealthy state. Thus, the results establish a baseline for the applicability of the piezoresistive stress sensor for an on-line monitoring PHM methodology.

1. Introduction

The piezoresistive silicon based stress sensor offers unique advantages, including direct measurement of the mechanical stresses and easy integration with existing systems. The sensor has demonstrated its capability of monitoring the stresses during the transfer molding process [1]. In Refs [2,3]., the evolution of the stresses in a package during the post mold curing process was investigated by the sensor. The underfill process was also studied by the sensor in Refs. [4,5]. The sensor was applied further to monitor the stresses during reliability testing. In Ref. [6], Roberts et al. studied the evolution of stresses during thermal cycling reliability tests. Similar results were presented by Shindler-Saefkow et al. [7] and Yu-Yao Chang et al. [8].

More recently, the sensor has been investigated for Prognostics and Health Monitoring (PHM) systems [9–12]. PHM has emerged as a promising solution to the need for more accurate life time prediction of new products that are more complex but have reduced development time. PHM combines in-situ measurements, data acquisition and interpretation of measured parameters, based on which the state of health of the electronic system can be assessed [13].

In this paper, the piezoresistive silicon based stress sensor is studied for a data driven approach to PHM. It has been shown that delamination can be detected by sensing the signal change of the sensor [14]. However, a systematic study about how different failures can influence the sensor output is missing. FEM analysis is conducted to fill this gap. First, various failure modes are introduced into a predictive model and the response of the sensor is investigated.

Collected data is then used to study the applicability of statistical pattern recognition algorithms. Three different algorithms are studied: Mahalanobis Distance (MD) [15] and Singular Value Decomposition (SVD) [16,17] for damage detection and Support Vector Machines (SVM) for damage typology [18]. The applicability of these algorithms to the current problem is discussed.

2. Stress sensor

This study focuses on an application of piezoresistive silicon-based stress sensor, called IForce. In this section the general working principle and construction of the sensor are presented.

The sensing elements are created by the channels of MOSFET transistors that are oriented in such a way that the change in stress is changing their resistivity. By measuring the currents flowing through the sensor in-plane shear stress, σ_{xy}, and difference in in-plane normal stress components, $\sigma_{xx} - \sigma_{yy}$, can be calculated from the following relations:

* Corresponding author.
E-mail address: Alicja.Palczynska@de.bosch.com (A. Palczynska).

http://dx.doi.org/10.1016/j.microrel.2017.04.011

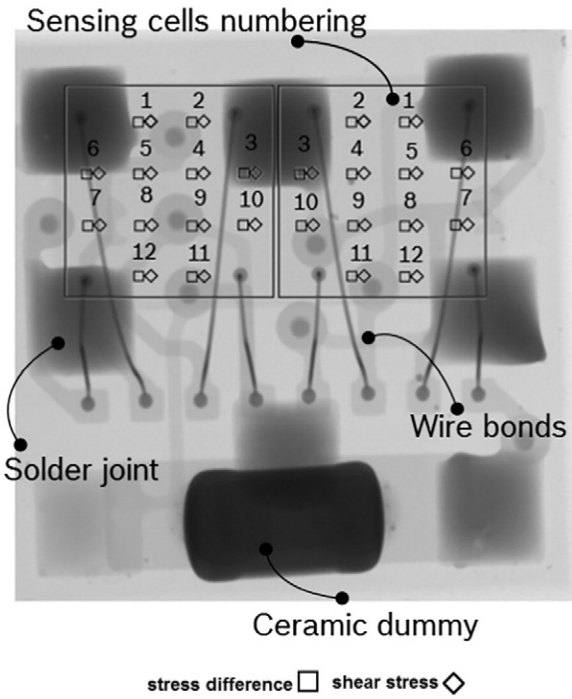

Fig. 1. X-Ray image of stress sensor used in this study.

$$\sigma_{xy} = \frac{1}{\pi_{11}^{n} - \pi_{12}^{n}} \frac{I_{OUT} - I_{IN}}{I_{OUT} + I_{IN}} \quad (1)$$

$$\sigma_{xx} - \sigma_{yy} = \frac{1}{\pi_{44}^{p}} \frac{I_{OUT} - I_{IN}}{I_{OUT} + I_{IN}} \quad (2)$$

where:

π_{11}, π_{12}, π_{44} – piezoresistive coefficients of silicon

I_{IN}, I_{OUT} – currents measured at the input and output of the sensor, respectively.

The use of MOSFET technology enables the stress measurements with high spatial resolution. In each sensor there is a whole matrix of sensing cells. The sensor with 24 sensing cells is used in the test, being placed in two 4 × 4 array. The cells in the corners of 4 × 4 arrays are inactive. The X-Ray image of sensor used in this study is shown in Fig. 1, where cell placements are marked with numbers.

The silicon die is packaged in a standard microelectronic LGA package, which is widely used to encapsulate a Hall sensor. Construction of the package is presented in Fig. 2. The silicon die is attached to a PCB using a die attach adhesive. Electrical connections are formed by wire bonds. There is also a dummy ceramic component soldered on the PCB. The whole construction is overmolded with commercially available epoxy molding compound. The final dimension of the package is 3 mm × 3 mm × 1 mm.

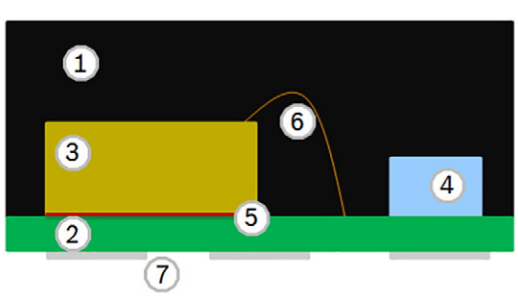

Fig. 2. Construction of LGA Package. 1 – mold, 2 – PCB, 3 – stress sensor, 4 – ceramic, 5 – die attach, 6 – wire bond, 7 – soldering pads.

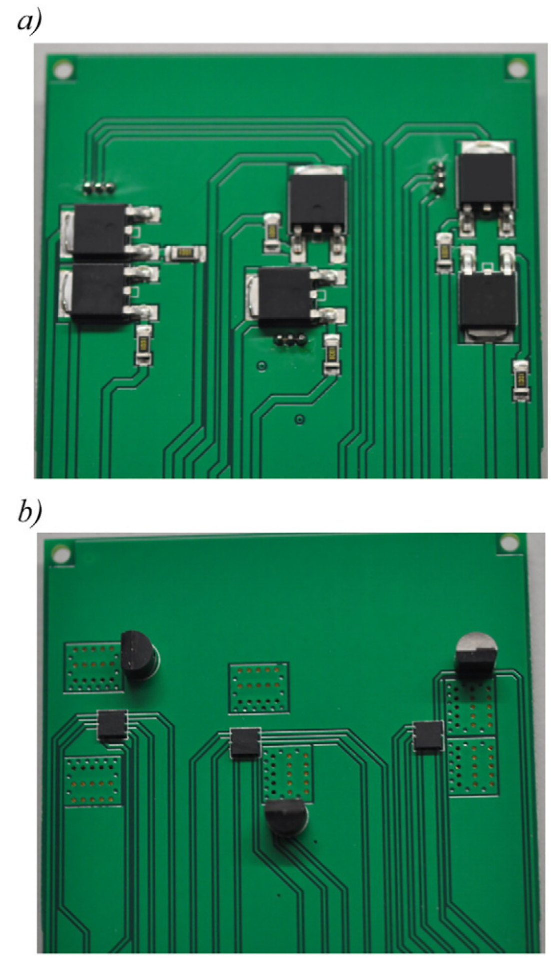

Fig. 3. Test vehicle a) top side view b) bottom side view.

3. Test vehicle

The test vehicle with stress sensors is a four full copper layer PCB containing six DPAK packages on one side (Fig. 3a) and three stress sensors on the other (Fig. 3b). This test vehicle is designed for reliability testing in which data acquisition from the sensors continues until the failure occurs.

The DPAK packages are placed in pairs at three different positions on the PCB. Two pairs are located along the edges of the PCB. The DPAKs within these two pairs have different relative orientations and the orientation toward the edges of PCB. The goal of this design is to

Table 1
Material properties.

Material properties considered in the simulation		Modulus of elasticity [MPa]	CTE [ppm/K]	Material law
DPAK	Copper lead frame	125,000	17	*Linear-elastic*
	Solder	49,551	20	*Viscoplastic*
	Silicon die	167,000	8	*Linear-elastic*
	Molding compound	17,000	12	*Viscoelastic*
PCB	Copper (PCB traces)	80,000	17	*Linear-elastic*
	Prepreg	24,000	14	*Viscoelastic*
Stress sensor	Substrate	23,000	19	*Homogenized*
	Adhesive	8000	51	*Viscoelastic*
	Silicon die	167,000	8	*Linear-elastic*
	Molding compound	26,000	8	*Viscoelastic*

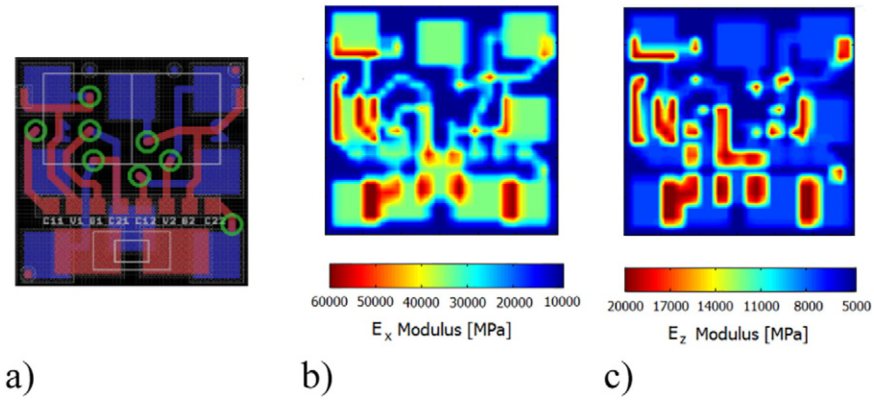

Fig. 4. a) Sensor PCB layout b) calculated homogenized Young's modulus values in x-direction c) in y-direction.

investigate the influence of the orientation of the package on the stress state inside it.

The stress sensors are placed underneath each DPAK pair where the highest temperature during active operation is expected. These are the locations where the largest load occurs during reliability testing, thus the failure is likely to occur first. Hence, it is the main region of interest, as the ultimate goal is to detect the failure that occurs in DPAK package.

4. FEM model

For numerical simulations presented in this work a commercial FEM code ANSYS® was used. To obtain quantitative results, the model must be prepared very carefully. The important steps of model preparation are described in this section.

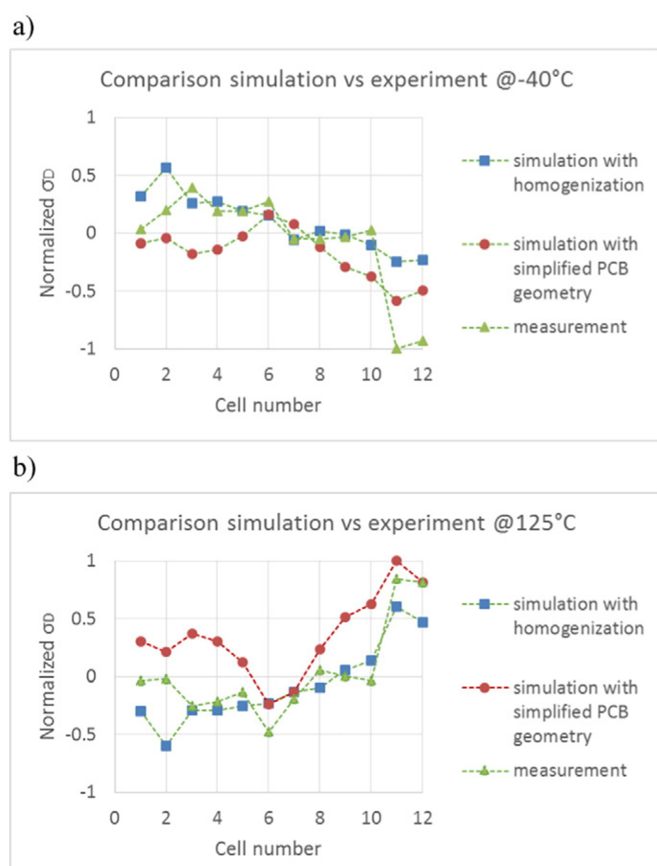

Fig. 5. Stress measurement vs. simulation.

First of all, all the material properties must be assessed. The material characterization started with detailed DMA measurements of the molding compound, which is an epoxy based thermosets type. Then, the linear viscoelastic material model is created and implemented in the model. Composite materials like PCB's were characterized as well by measuring the prepreg and copper foils separately. In the global model a solder and a wire bond were modelled using linear elastic properties, because it would be computationally too expensive to use the model considering non-linear properties. The material properties used are presented in Table 1.

Additionally, a detailed geometry must be taken into account. In this simulation especially the internal geometry of the stress sensor must be very accurate. This includes also the layout of the PCB within the sensor package. To simulate the exact geometry is computationally too expensive, as the PCB layout contains very small elements. Thus, the PCB inside the senor package was modelled using homogenization technique [19]. This was accomplished in two stages. First, the local properties of the prepreg and copper layer were calculated for each cell separately using linear rules of mixture. Effective values were computed as an average of properties of the individual phases according to their volume fractions. Then, the layer specific formulation of the PCB, consisting of insulating and copper layers containing layout was converted into homogenous block in the thickness direction. An example of calculated effective Young's modulus distribution is shown in Fig. 4. The results from simulation, that takes the layout into account, are validating the measurements much better as shown in Fig. 5.

The simulation was done for a passive temperature cycle performed between −40 °C and 125 °C. The out of plane deformation obtained from structural simulation at 125 °C is presented in Fig. 6. The test vehicle bends visibly along longer edge, having the largest deformation in the middle of the PCB.

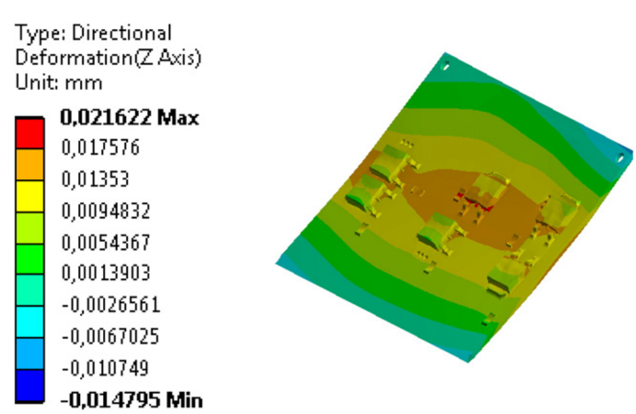

Fig. 6. Global PCB deformation at 125 °C.

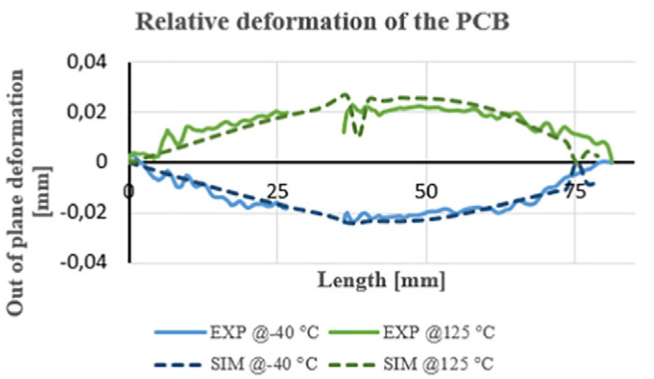

Fig. 7. Warpage measurement and simulation comparison, passive cycling at −40 °C and 125 °C evaluated along a diagonal.

The simulations results were validated globally utilizing warpage measurements. The deformation of the test vehicle was measured using Digital Image Correlation (DIC). The results of out of plane deformation are evaluated along the diagonal and compared with the numerical prediction in Fig. 7. The results correlate very well with results of experiments.

5. Failure modes

In order to investigate the influence of different failures on the sensor response, they were inserted explicitly into the validated FEM simulation, as a part of geometry. Here, three failure modes were investigated. The schematic pictures with the areas, where the failures were inserted, are marked in orange, are presented in Fig. 8. First of the investigated failure modes was delamination in the area of the sensor as shown in Fig. 8a. This failure should give the biggest response of a sensor. The second one was delamination in the DPAK area (Fig. 8b) to investigate if the failure not placed directly under the sensor can be detected. The third inserted failure mode is a solder crack under the sensor (Fig. 8c). This failure is inserted in such a way that does not affect electrical connections of the sensor. The inserted failures and the reference names used later in this paper are summarized in Table 2. This work focuses on detecting different damage types. Considerations about damage size are beyond scope of this paper.

6. Statistical pattern recognition techniques

In this section used pattern recognition techniques are described, together with practical application on the data gathered from simulation.

Table 2
Investigated failure modes.

FM1	Delamination in the sensor area
FM2	Delamination in the DPAK area
FM3	Solder crack in sensor area

Three algorithms were applied – Mahalanobis distance, Singular Value Decomposition and Support Vector Machine. Both methodologies begin with gathering the sensor data i.e. values of stress difference and shear stress at the 24 sensor cells locations as shown in Fig. 9. These values will be referred to as performance parameters.

To apply the statistical pattern recognition techniques, the information about the variability of sensor response is needed. For this purpose the uncertainties present in experiment are assessed [20]. After evaluation of the simulation results, it was stated that the sample to sample variability is too high to detect failure in a reliable way. Thus, only the variability related to the measurement process itself is taken into account in the process of creating the statistical distribution. That means, a database of healthy results was created as a normal distribution with standard deviation of 0.3 MPa for both stress difference and shear stress values.

6.1. Mahalanobis distance

Mahalanobis distance is defined as a distance in multidimensional space that considers correlations among parameters [21]. The MD value is calculated using the normalized value of performance parameters, which eliminates the problem of scaling. It is different than Euclidean distance, because it takes into account also correlation coefficients of performance parameters, which is the reason for the algorithm's sensitivity.

In this approach a healthy baseline and a threshold are needed to classify a product to be healthy or unhealthy. The performance parameters are stored in a matrix X_{ij} with elements denoted as x_{ij} (Fig. 9), where $i = 1, 2, \ldots, p$ and p is the total number of performance parameters (here $p = 24$) and $j = 1, 2, \ldots, m$ where m is the total number of observations. The normalized values are calculated as follows:

$$z_{ij} = \frac{x_{ij} - \overline{x}_i}{s_i} \tag{3}$$

where:

$$\overline{x}_i = \frac{1}{m}\sum_{j=1}^{m} x_{ij} \tag{4}$$

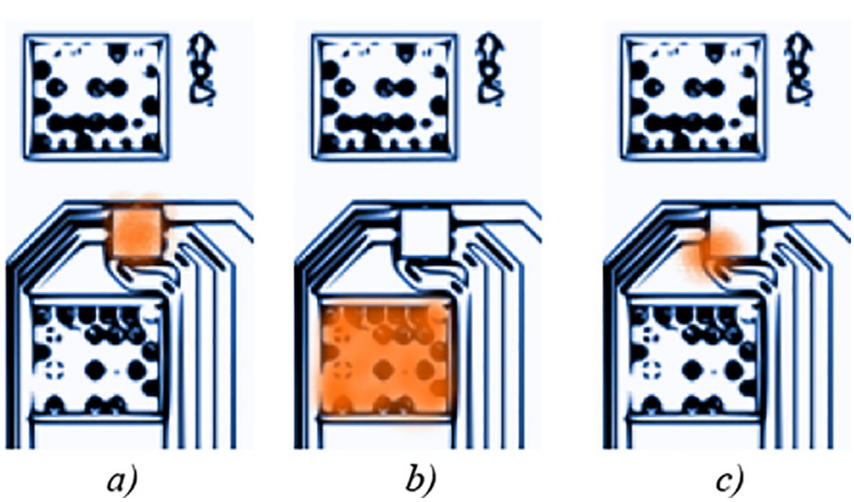

Fig. 8. Locations of the inserted failure modes.

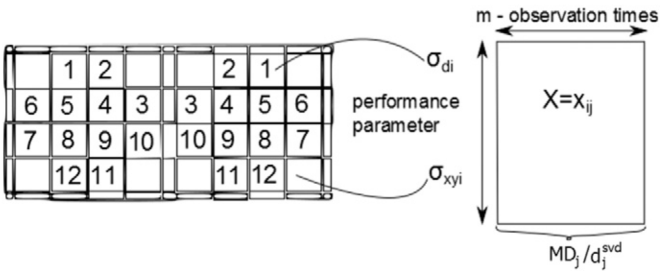

Fig. 9. Input matrix construction for both algorithms.

$$s_i = \sqrt{\frac{\sum_{j=1}^{m} (x_{ij} - \overline{x}_i)^2}{m-1}} \quad (5)$$

The correlation matrix is calculated as:

$$C = \frac{1}{m-1} \sum_{j=1}^{m} Z_j Z_j^T \quad (6)$$

Finally, the MD for a healthy dataset is calculated as:

$$MD_j = \frac{1}{p} Z_j^T C^{-1} Z_j \quad (7)$$

After calculating the MD values for each observation from healthy baseline, it is needed to establish a threshold to make a decision between healthy and damaged state. For threshold determination a probabilistic approach is used. Since the MD are not normally distributed a Box-Cox transformation [21] is used. It converts the variable which contains only positive values and does not follow normal distribution into normally distributed variable. Then, the determination of a threshold can be done based on a mean (μ_x) and a standard deviation (σ_x) of the transformed MD variable. As higher MD values are the ones that indicate failure, only the upper part of the control chart is significant for this approach. A warning limit threshold is defined as ($\mu_x + 2\sigma_x$) and a fault alarm threshold as ($\mu x + 3\sigma_x$).

A result of fault classification conducted with MD approach is presented in Fig. 10. The first hundred points are from the healthy baseline and the last data point contains damage. It is clearly detected, crossing the fault alarm threshold. However, some of the points from healthy baseline are crossing the warning level. It is caused by the threshold definition – about 98% of points should lay within the ($\mu_x + 2\sigma_x$) bound. To deal with this property, in the real time measurements, a couple of consecutive points should be classified as potentially containing failure, to give actual the warning.

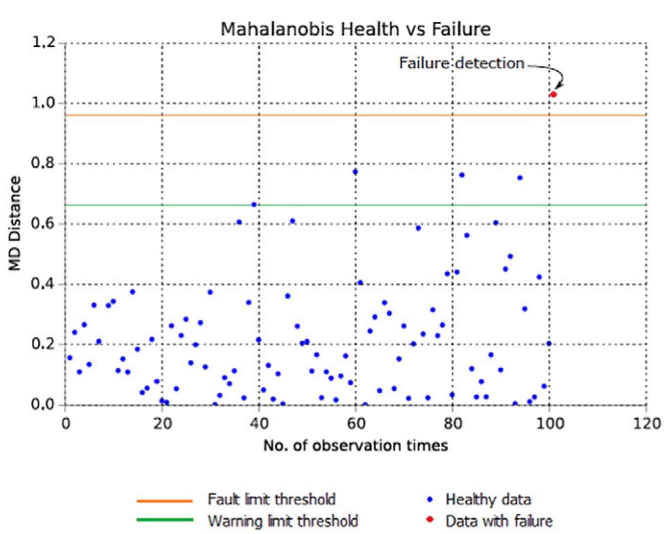

Fig. 10. Results of MD algorithm.

Table 3
Damage detection by MD algorithm for different failure modes and stress components.

Failure mode	σ_D	σ_{XY}
FM1 (delamination/sensor)	✓	✓
FM2 (delamination/DPAK)	✓	✘
FM3 (solder crack)	✓	✓

The detection results for all failure modes using both stress difference and shear stress data are presented in Table 3. It shows that this method works very well in detecting failure for different damage types. Only in case of damage recognition based on shear stress values the results are not always conclusive.

The main advantage of this method is that it doesn't require knowledge of failure modes for training. That means the only thing needed to start the algorithm is a healthy baseline that can be created based on the initial measurements in the system. Another advantage it is represented by the fast calculation algorithm. In conclusion it can be stated that this method can easily be used for damage detection. Although, for a robust algorithm it must be further improved.

6.2. Singular value decomposition

Singular Value Decomposition is a discrete version of the algorithm known as Proper Orthogonal Decomposition (POD). It is a multi-variate statistical method for data analysis. Its primary use is order reduction as it enables projection of high-dimensional data into lower dimensional space [20]. What is more interesting for this work, it offers also feature

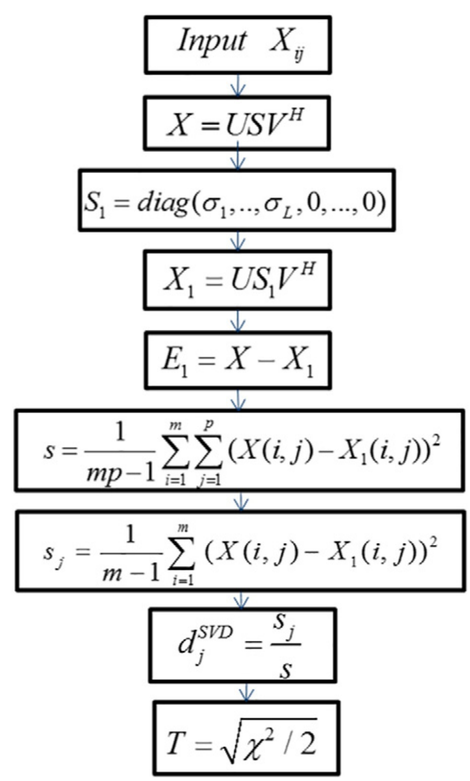

Fig. 11. The SVD algorithm workflow [21].

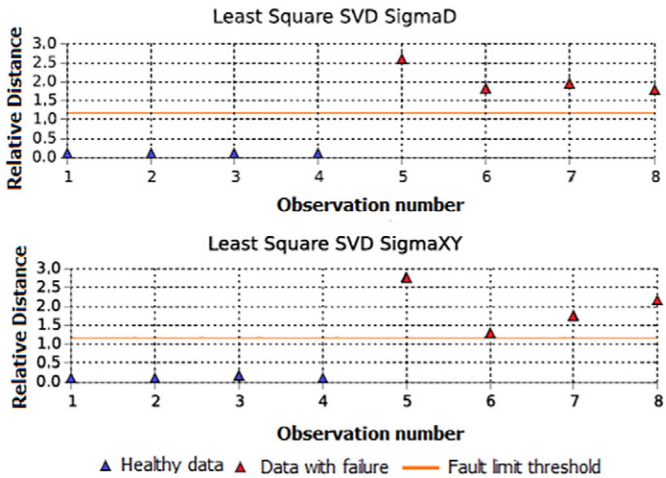

Fig. 12. The least square SVD results.

extraction from the data, by unveiling its structure. The main idea here is to decompose the matrix into a product:

$$X_{ij} = USV^T \quad (8)$$

where U and V are two orthonormal matrices and S contains the singular values σ of the matrix X_{ij}. When the matrix X_{ij} contains data with damage, the decomposition deviates from the one calculated only with data from intact structures.

The SVD algorithm workflow used in this work is presented in Fig. 11 [21]. The first step is to create a performance parameter space. The matrix X_{ij} is built in the same way as for MD approach. A condition that has to be fulfilled to implement this method is that the number of observations containing damage must be bigger or equal to number of healthy observations. In this case, a matrix with eight columns is created, four first columns contain healthy data and the rest data with damage. Next, the matrix is decomposed according to formula (7). Then all the singular values below arbitrary chosen noise level are set to zero and a matrix X_1 is resynthesized. Afterwards, the residual matrix E_1, the standard deviation of residuals and standard deviation of every observation are computed. Finally, the relative distance d_j is obtained, which follows χ^2 distribution with mean $m = 1$. The threshold for fault qualification is determined based on standard deviation σ of this distribution with confidence level 95%.

Using this procedure, an automatic classification between damaged and healthy observations can be made. The problem with the classical least-squares SVD technique is that it is very sensitive to outliers [22].

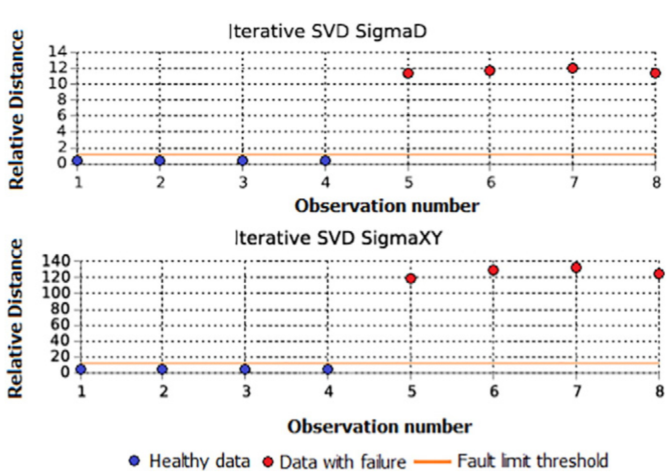

Fig. 13. The iterative SVD results.

Table 4
Normalized calculation time of used algorithms.

Type	Calculation time (normalized)
Mahalanobis distance	1
Classic SVD	0.025
Iterative SVD	0.039

To reduce the outliers influence an iterative SVD can be used. In this approach first the classical least-squares SVD algorithm is applied. Then the observations with outlying distance d_j are eliminated and the SVD of the remaining observations is calculated again.

In Fig. 12 an example of output of classical least square SVD and in Fig. 13 of iterative SVD is presented. The damage is detected for both classical and iterative SVD. These methods were tested on data concerning all three failure modes and in all cases the damage was detected. It is also worth to notice, that the iterative SVD gives much sharper separation of the healthy and damaged observations. The main advantage of this approach is short calculation time. As shown in Table 4 both classic and iterative SVD have a calculation time much shorter than in case of Mahalanobis distance. Similarly to previous method it does not require the prior knowledge about the failure modes and works on normalized data. The main disadvantage here is that the requirement for damage detection is to have multiple observations containing failure.

The advantages and disadvantages of both presented methods are summarized in Table 5.

Support vector machine

Support Vector Machines is a machine learning algorithm that can solve classification problems. It is very popular because it can form accurate boundaries between dataset even with small amount of training data [23]. Additionally, it often gives a good generalization and finds a single global minimum for a problem. The main idea behind it is to find the plane separating the two datasets in such a way that the distance between them is maximized. For n-dimensional sets of data, a n-1-dimensional hyperplane that separates them is searched. This hyperplane boundary can have linear or nonlinear character.

To explain the SVM algorithm, an example of two dimensional linear problem is presented (Fig. 14). First, the training data are labeled, creating the sets. For each point x_i from the first data set the value $y_i = -1$ and for those from the other set the value $y_i = 1$ is assigned. The classification in this case is performed by considering plane $H1$ that consist of the points which satisfy the equation $wx + b = 0$, where w is normal to the plane and b is the perpendicular distance from the plane to the origin, normalized by length of w. The following conditions should be satisfied for all training data points:

$$x_i \cdot w + b \geq 1 \qquad for \;\; y_i = 1 \quad (9)$$

Table 5
Advantages and disadvantages of tested damage detection algorithms.

Mahalanobis distance	SVD
Advantages	
Works on normalized data	Works on normalized data
Relatively long calculation time	Short calculation time
Does not require prior knowledge about failures	Does not require prior knowledge about failures
Good accuracy	
Easy to implement	
Disadvantages	
inconclusive for shear stress results	Sensitive to noise
False warning result	Requires more than one data point for data with failure

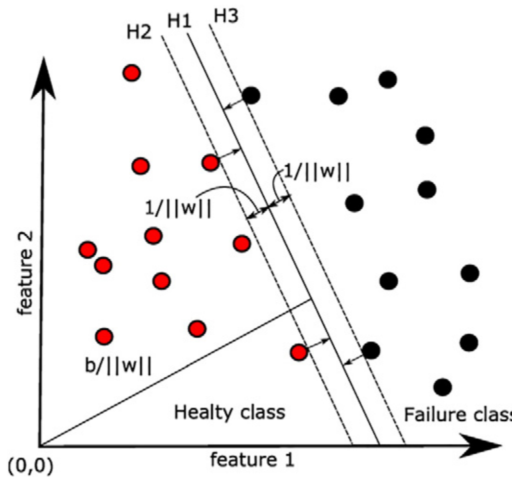

Fig. 14. Linear SVM problem.

$$x_i \cdot w + b \le -1 \quad for\ \ y_i = -1 \tag{10}$$

The points for which the equality (8) is satisfied, lay on the hyperplane *H2* and the points for which the equality (9) is satisfied lay on the hyperplane *H3*. Hence, the distance between *H1* and *H2* is $d_+ = 1/||w||$, the distance between *H1* and *H3* is $d_- = 1/||w||$, and the margin is simply $2/||w||$. Considering that *H2* and *H3* are parallel and no points lie between them, the optimization problem needs to minimize $||w||^2$, which is subjected to constraint:

$$y_i(x_i w + b) - 1 \ge 0 \tag{11}$$

Eq. (10) simply combines the equalities (8) and (9) into one set of inequalities.

The optimization problem is then solved by changing the constraints into Lagrangian multipliers. The objective function can be written as [23]:

$$L_p = \frac{1}{2}\|w^2\| - \sum_{i=1}^{m} \alpha_i y_i (x_i w + b) + \sum_{i=1}^{m} \alpha_i \tag{12}$$

where α_i are positive Lagrangian multipliers.

The aim is to minimize L_p with respect to w and b.

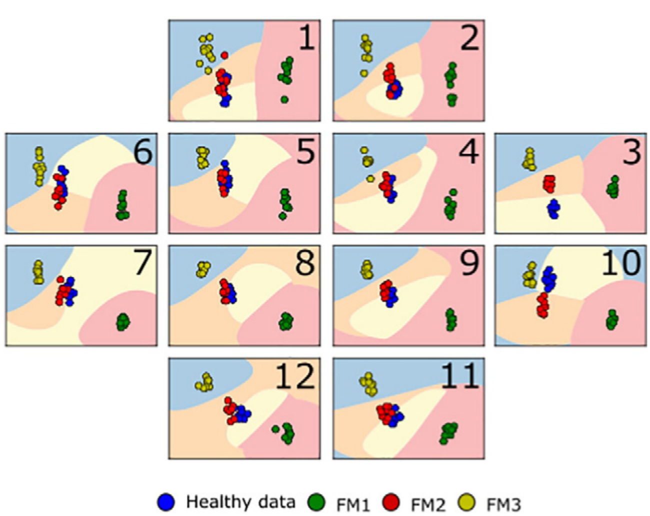

Fig. 15. Results of SVM algorithm with RBF kernel function calculated separately for every cell.

The non-linear classification involves mapping the data points from a lower dimensional feature space into a higher dimensional space. This can be made by a function which is called a kernel function. There are several functions used in the literature, but the one used in this study is the Gaussian radial basis function (RBF):

$$K(x_i, x_j) = \exp\left(-\frac{\|x-y\|^2}{2\sigma^2}\right) \tag{13}$$

After mapping the points, the same linear separation procedure is applied just in a different space.

For our problem this method is applied to each sensor cell separately. The training data contains healthy and failure information, such as the stress difference and shear stress. The results are depicted in Fig. 15. They show the influence of damage to each sensor cell. Different colored areas are specifying the range in which a data point will be classified as one of the four states – yellow for healthy, red for FM1, orange for FM2 and blue for FM3. The data sets containing different failures are separated very well. Only in case of FM2 in some cells the points are not perfectly separated from healthy data. If the point is already identified as containing failure, by one of the previous methods, then the wrong qualification by SVM only between one of the failures and the healthy data can be easily avoided by not taking into account the healthy data as a training set. That's the reason why this method is proposed only for damage typology, not for damage detection.

7. Conclusions

In this work, damage detection using the piezoresistive silicon stress sensor was studied. The stress states in the sensor subjected to different damage types was collected using validated FEM simulations. Then, three statistical pattern recognition algorithms were investigated with the data - Mahalanobis distance and Singular Value Decomposition for damage detection and Support Vector Machine for damage typology. Both damage detection algorithms have successfully distinguished the differences between healthy and damage data, even for the case that the failure was inserted not directly under the sensor. The advantages and disadvantages of both algorithms were evaluated. The Support Vector Machine was applied to classify the failures.

It is recommended to conduct in the future a broader study to evaluate the minimum size of failure that can be detected by the sensor. Additionally, the actual damage data of test vehicles should be collected to evaluate the performance of the proposed approach.

References

[1] T. Schreier-Alt, K. Unterhofer, F. Ansorge, K. Lang, Stress analysis during assembly and packaging, Components and Technology Conference (ECTC), 2011 (IEEE 61st, vol., no., pp.16841690, May 31 2011–June 3 2011).

[2] Y. Zou, J.C. Suhling, R.W. Johnson, R.C. Jaeger, A.K.M. Mian, In-situ stress state measurements during chip-on-board assembly, Electronics Packaging Manufacturing, 1999 (IEEE Transactions on, vol.22, no.1, pp.38,52, Jan).

[3] P. Gromala, S. Fischer, T. Zoller, A. Andreescu, J. Duerr, M. Rapp, J. Wilde, Internal stress state measurements of the large molded electronic control units, Thermal, Mechanical and Multi-Physics Simulation and Experiments in Microelectronics and Microsystems (EuroSimE), 2013 (14th International Conference on, vol., no., pp.1,8, 14–17 April 2013).

[4] F. Schindler-Saefkow, F. Rost, A. Schingale, D. Wolf, B. Wunderle, J. Keller, M. Michel, S. Rzepka, Measurements of the mechanical stress induced in flip chip dies by the underfill and simulation of the underlying phenomena of thermal-mechanical and chemical reactions, Electronics System-Integration Technology Conference (ESTC), 2014 (vol., no., pp.1,6, 16–18 Sept. 2014).

[5] G. Schlottig, F. Schindler-Saefkow, J. Zurcher, B. Michel, T. Brunschwiler, Sequentially formed underfills: Thermo-mechanical properties of underfills at full filler percolation, Electronics Packaging Technology Conference (EPTC), 2013 (2013 IEEE 15th, vol., no., pp.560,564, 11–13 Dec).

[6] J.C. Roberts, M.K. Rahim, S. Hussain, J.C. Suhling, R.C. Jaeger, P. Lall, Die stress variation in area array components subjected to accelerated life testing, Thermal and Thermomechanical Phenomena in Electronic Systems, 2008 (ITHERM 2008. 11th Intersociety Conference on, vol., no., pp.705–713, 28–31 May 2008).

[7] F. Schindler-Saefkow, F. Rost, A. Otto, W. Faust, B. Wunderle, B. Michel, S. Rzepka, Stress chip measurements of the internal package stress for process characterization

and health monitoring, Thermal, Mechanical and Multi-Physics Simulation and Experiments in Microelectronics and Microsystems (EuroSimE), 2012 (13th International Conference on, vol., no., pp.1/10–10/10, 16–18 April 2012).
[8] Y.Y. Chang, H. Chung, B.J. Lwo, K.F. Tseng, In situ stress and reliability monitoring on plastic packaging through piezoresistive stress sensor, Components, Packaging and Manufacturing Technology, 2013 (IEEE Transactions on, vol.3, no.8, pp.1358–1363, Aug).
[9] A. Palczynska, F. Pesth, P.J. Gromala, T. Melz, D. Mayer, Acquisition unit for in-situ stress measurements in smart electronic systems, Thermal, Mechanical and Multi-physics Simulation and Experiments in Microelectronics and Microsystems (Eurosime), 2014 (15th international conference on, vol., no., pp.1–4, 7–9 April 2014.
[10] B. Wu, D.S. Kim, B. Han, A. Palczynska, P.J. Gromala, Thermal deformation analysis of automotive electronic control units subjected to passive and active thermal conditions, Thermal, Mechanical and Multi-Physics Simulation and Experiments in Microelectronics and Microsystems (EuroSimE), 2015 (16th International Conference on, vol., no., pp.1–6, 19–22 April 2015).
[11] M.K. Rahim, J. Roberts, J.C. Suhling, R.C. Jaeger, P. Lall, Continuous in-situ die stress measurements during thermal cycling accelerated life testing, Electronic Components and Technology Conference, 2007 (ECTC '07. Proceedings. 57th, vol., no., pp.1478–1489, May 29 2007–June 1 2007).
[12] A. Palczynska, B. Wu, D.S. Kim, P. Gromala, B. Han, D. Mayer, T. Melz, Application of the IForce piezoresistive silicon based stress sensor for prognostic and health monitoring methods, Microelectronics Packaging Conference (EMPC), 2015 (European, vol., no., pp.1–6, 14–16 Sept. 2015).
[13] M. Pecht, B. Tuchband, N. Vichare, Q.J. Ying, Prognostics and health monitoring of electronics, Thermal, Mechanical and Multi-Physics Simulation Experiments in Microelectronics and Micro-Systems, 2007 (EuroSime 2007. International Conference on, vol., no., pp.1–8, 16–18 April 2007).
[14] P. Gromala, A. Palczynska, B. Han, Prognostic approaches for the wirebond failure prediction in power semiconductors: a case study using DPAK package, Electronic Packaging Technology (ICEPT), 2015 (16th International Conference on, vol., no., pp.413–418, 11–14 Aug. 2015).
[15] P. Lall, P. Choudhary, S. Gupte, Health monitoring for damage initiation & progression during mechanical shock in electronic assemblies, Proceedings of the 56th IEEE Electronic Components and Technology Conference, San Diego, California 2006, pp. 85–94 (May 30–June 2).
[16] R. Ruotolo, C. Surace, Using SVD to detect damage in structures with different operational conditions, Journal of Sound and Vibration, Volume 226, 23 September 1999, pp. 425–439 (Issue 3). (ISSN 0022-460X).
[17] R. Hajrya, N. Mechbal, M. Verge, Proper orthogonal decomposition applied to structural health monitoring, Communications, Computing and Control Applications (CCCA), 2011 (International Conference on, vol., no., pp.1–6, 3–5 March 2011).
[18] B. Saha, S. Poll, K. Goebel, J. Christophersen, An integrated approach to battery health monitoring using bayesian regression and state estimation, Autotestcon, 2007 IEEE, Baltimore, MD 2007, pp. 646–653.
[19] E. Zukowski, T. Kimpel, D. Kraetschmer, A. Roessle, Efficient modeling of printed circuit boards structures for dynamic simulations, Thermal, Mechanical and Multi-Physics Simulation and Experiments in Microelectronics and Microsystems (EuroSimE), 2015 (16th International Conference on, vol., no., pp.1–5, 19–22 April 2015).
[20] A. Palczynska, F. Schindler-Saefkow, P. Gromala, K. Kreyßig, S. Rzepka, D. Mayer, T. Melz, Investigation of uncertainty sources of piezoresistive silicon based stress sensor, Appl. Mech. Mater. 807 (2015) 45–54.
[21] S. Vanlanduit, E. Parloo, B. Cauberghe, P. Guillaume, P. Verboven, A robust singular value decomposition for damage detection under changing operating conditions and structural uncertainties, J. Sound Vib. 284 (3–5) (21 June 2005) 1033–1050 (ISSN 0022-460X).
[22] S. Kumar, T.W.S. Chow, M. Pecht, Approach to fault identification for electronic products using Mahalanobis distance, Instrumentation and Measurement, 2010 (IEEE Transactions on, vol.59, no.8, pp.2055–2064, Aug).
[23] C.J.C. Burges, A tutorial on support vector machines for pattern recognition, Data Mining and Knowledge Discovery, Volume 2, 1998, p. 121 (Number 2).